Supplementary Material for the paper entitled:

Stabilization of 2-pyridyltellurium(II) derivatives by oxidorhenium(V) complexes

Felipe Dornelles da Silva,[1] Maximilian Roca Jungfer,[2] Adelheid Hagenbach,[2] Ernesto Schulz Lang[1], and Ulrich Abram[2*]*

[1] Universidade Federal de Santa Maria, Department of Chemistry, Avenida Roraima, nº 1000, Santa Maria, Rio Grande do Sul, Brazil.
E-mail: eslang@ufsm.br

[2] Freie Universität Berlin, Institute of Chemistry and Biochemistry, Fabeckstr. 34/36, 14195 Berlin, Germany
E-mail: ulrich.abram@fu-berlin.de

1. Crystallographic data **4**

Table S1. Crystallographic data and data collection parameters 4

Figure S1. Structure of $(CF_3pyTe)_2$ (**1**). Ellipsoid plot with thermal ellipsoids representing 50 per cent probability and unit cell plot illustrating secondary Te…Te bonds of 3.802 Å, intermolecular Te…N contacts of 3.270 Å and a weak intermolecular H bond of 2.590 Å 7

Table S2. Selected bond lengths (Å) and angles (°) in $(CF_3pyTe)_2$ (**1**). 7

Figure S2. Ellipsoid representation of the molecular structure of $(HCF_3py)TeCl_2$ (**2**). Thermal ellipsoids represent 50 per cent probability 7

Table S3. Selected bond lengths (Å) and angles (°) in $(HCF_3py)TeCl_2$ (**2**). 7

Figure S3. Ellipsoid representation of the molecular structure of $(HCF_3py)TeBr_2$ (**3**). Thermal ellipsoids represent 50 per cent probability 8

Table S4. Selected bond lengths (Å) and angles (°) in $(HCF_3py)TeBr_2$ (**3**). 8

Figure S4. 'Long-range' Te-Br interactions in $(HCF_3py)TeBr_2$ (**3**) 8

Figure S5. Ellipsoid representation of the molecular structure of $[ReO_2Cl(pyTeCl)(PPh_3)_2]$ (**5**). Thermal ellipsoids represent 50 per cent probability. 9

Table S5. Selected bond lengths (Å) and angles (°) in $[ReO_2Cl(pyTeCl)(PPh_3)_2]$ (**5**) 9

Figure S6. Ellipsoid representation of the molecular structure of $[ReO_2Cl(CF_3pyTeCl)(PPh_3)_2]$ (**4**) x 3 DMF. Thermal ellipsoids represent 50 per cent probability. 10

Table S6. Selected bond lengths (Å) and angles (°) in $[ReO_2Cl(CF_3pyTeCl)(PPh_3)_2]$ (**4**) 10

2. Spectroscopic Data **11**

Figure S7. IR spectrum of bis(5-trifluoromethyl-2-pyridyl)ditellane (**1**) 11

Figure S8. Raman spectrum of bis(5-trifluoromethyl-2-pyridyl)ditellane (**1**) 11

Figure S9. ^{1}H NMR spectrum of bis(5-trifluoromethyl-2-pyridyl)ditellane (**1**) in $CDCl_3$ 12

Figure S10. ^{13}C NMR spectrum of bis(5-trifluoromethyl-2-pyridyl)ditellane (**1**) in $CDCl_3$ 12

Figure S11. ^{19}F NMR spectrum of bis(5-trifluoromethyl-2-pyridyl)ditellane (**1**) in $CDCl_3$ 13

Figure S12. ^{125}Te NMR spectrum of bis(5-trifluoromethyl-2-pyridyl)ditellane (**1**) in $CDCl_3$ 13

Figure S13. IR spectrum of $(HCF_3py)TeCl_2$ (**2**). 14

Figure S14. Raman spectrum of $(CF_3pyH)TeCl_2$ (**2**). 14

Figure S15. IR spectrum of $(HCF_3py)TeBr_2$ (**3**). 15

Figure S16. Raman spectrum of (HCF3py)TeBr2 (3).

Figure S17. IR spectrum of $[ReO_2Cl(CF_3pyTeCl)(PPh_3)_2]$ (**4**). 16

Figure S18. Raman spectrum of $[ReO_2Cl(CF_3pyTeCl)(PPh_3)_2]$ (**4**) 16

Figure S19. ^{19}F NMR spectrum of $[ReO_2Cl(CF_3pyTeCl)(PPh_3)_2]$ (**4**). 17

Figure S20. ^{31}P NMR spectrum of $[ReO_2Cl(CF_3pyTeCl)(PPh_3)_2]$ (**4**). 17

Figure S21. IR spectrum of $[ReO_2Cl(pyTeCl)(PPh_3)_2]$ (**5**). 18

Figure S22. Raman spectrum of $[ReO_2Cl(pyTeCl)(PPh_3)_2]$ (**5**). 18

Figure S23. ^{31}P NMR spectrum of $[ReO_2Cl(pyTeCl)(PPh_3)_2]$ (**5**) 19

Figure S24. ^{125}Te NMR spectrum of $[ReO_2Cl(pyTeCl)(PPh_3)_2]$ (**5**). 19

3. Computational Chemistry **20**

Table S7. Results of the charge analysis for selected atoms in $[ReO_2Cl(pyTeCl)(PPh_3)_2]$ (**5**). Wiberg bond order matrix for selected atoms, relevant bond orders are bold 20

Table S8. Lone-pair decomposition of Re and Te in $[ReO_2Cl(pyTeCl)(PPh_3)_2]$ (**5**). 20

Table S9. Natural electron configuration of selected atoms in $[ReO_2Cl(pyTeCl)(PPh_3)_2]$ (**5**). 20

Table S10. Selected parameters from the second order perturbation analysis of $[ReO_2Cl(pyTeCl)(PPh_3)_2]$ (**5**). Delocalization, which was interpreted as an ionic bond is bold. 21

Table S11. Three-centered *trans*-bonds around Re (3c4e hyper-bonds) in $[ReO_2Cl(pyTeCl)(PPh_3)_2]$ (**5**). 21

Figure S25. Donation of lone pair 1 (LP1) of O2 into empty valence orbital 1 (LV1) of Re and Te in $[ReO_2Cl(pyTeCl)(PPh_3)_2]$ (**5**) based on the NBO analysis. The isosurfaces are shown with an isosurface value of 0.08 21

Figure S26. Donation of lone pair 2 (LP2) of O2 into empty valence orbital 1 (LV1) of Re and Te in

[$ReO_2Cl(pyTeCl)(PPh_3)_2$] (**5**) based on the NBO analysis. The isosurfaces are shown with an isosurface value of 0.08 22

Figure S27. Donation of lone pair 4 (LP4) of O2 into empty valence orbital 1 (LV1) of Re and Te in [$ReO_2Cl(pyTeCl)(PPh_3)_2$] (**5**) based on the NBO analysis. The isosurfaces are shown with an isosurface value of 0.08 22

Figure S28. Donation of lone pair 3 (LP3) of O2 into the antibonding Re-O1 orbital of [$ReO_2Cl(pyTeCl)(PPh_3)_2$] (**5**) based on the NBO analysis. LV1 of Te is also shown to visualize the orthogonality of the two orbitals and the absence of donation of LP3 of O2 into this orbital. The isosurfaces are shown with an isosurface value of 0.08. 23

Figure S29. Interbasin surfaces of Re-O2 and Te-O2 contacts in [$ReO_2Cl(pyTeCl)(PPh_3)_2$] (**5**). 23

Figure S30. Basins of Re and Te in [$ReO_2Cl(pyTeCl)(PPh_3)_2$] (**5**) with mapping of the electron density at the 0.06 isosurface value. The electron density at the surface is a measure of the bond strength 24

Figure S31. Basins of O2 and the superposition of Re, Te and O2 basins in [$ReO_2Cl(pyTeCl)(PPh_3)_2$] (**5**) with mapping of the electron density at the 0.06 isosurface value. The electron density at the surface is a measure of the bond strength 24

Table S12. Selected properties of the electron density at important bond critical points in [$ReO_2Cl(pyTeCl)(PPh_3)_2$] (**5**). 24

Figure S32. ELF with bond paths (black) in [$ReO_2Cl(pyTeCl)(PPh_3)_2$] (**5**). Cuts through a) the C=N bond in z direction to the pyridine plane, b) the O N contact in z direction to the pyridine plane, c) the Re-N dative bond in z direction to the pyridine plane, c) the Re-O bond in z direction to the pyridine plane or along the Re-P-O plane, e) the Re Te contact in z direction to the pyridine plane, f) the Te-C bond in z direction to the pyridine plane, g) the Te-O bond in z direction to the pyridine plane 25

Figure S33. Laplacian map of the electron density in [$ReO_2Cl(pyTeCl)(PPh_3)_2$] (**5**) (blue = negative; red = positive) with negative values corresponding to local electronic charge accumulation while positive values indicate regions of local electronic charge depletion. Cut through the Re Te contact in z direction to the pyridine plane 25

Figure S34. 3D Laplacian map of the electron density at the 0 (enclosure) level in [$ReO_2Cl(pyTeCl)(PPh_3)_2$] (**5**) showing regions of electronic charge accumulation 25

Figure S35. Gradient vector field of the electron density cut through the respective Te-O (left) and O-Re (right) bonds perpendicular to the Re-O-Te plane in [$ReO_2Cl(pyTeCl)(PPh_3)_2$] (**5**) mapped on the electron density iso contour lines with topological descriptors. (3,-3) = brown, (3,-1) = blue, (3,1) = orange, bond path between (3,-3) and (3,-1) critical points = cyan. Additionally, a contour line of the van der Waals radius (black) is shown 26

S4. References 26

1. Crystallographic data

The intensities for the X–ray determinations were collected on a STOE IPDS 2T or a Bruker Apex-II CCD with Mo Kα or Ag Kα radiation. The space groups were determined by the detection of systematical absences. Absorption corrections were carried out by integration methods or SADABS.[1,2]. Structure solution and refinement were performed with the SHELX program package on the OLEX-2 platform [3-5]. Hydrogen atoms were derived from the final Fourier maps and refined or placed at calculated positions and treated with the 'riding model' option of SHELXL. The representation of molecular structures was done using the program DIAMOND 4.2.2 [6].

Table S1: Crystallographic data and data collection parameters

	$(CF_3pyTe)_2$ (**1**)	$[HCF_3pyTeCl_2]$ (**2**)
Empirical formula	$C_{12}H_6F_6N_2Te_2$	$C_6H_4Cl_2F_3NTe$
Formula weight	547.39	345.60
Temperature/K	100	293(2)
Crystal system	monoclinic	trigonal
Space group	$P2_1/c$	R-3
a/Å	22.09(1)	21.905(3)
b/Å	6.006(1)	21.905(3)
c/Å	11.377(9)	11.071(1)
α/°	90	90
β/°	100.29(3)	90
γ/°	90	120
Volume/Å^3	1485(1)	4600(1)
Z	4	18
ρ_{calc}g / cm^3	2.448	2.245
μ / mm^{-1}	2.082	3.428
F(000)	1000	2880.0
Crystal size / mm^3	0.35 x 0.30 x 0.25	0.4 × 0.4 × 0.2
Radiation	AgKα (λ = 0.56086)	MoKα (λ = 0.71073)
2Θ range for data collection/°	4.436 to 47.22	9.304 to 49.942
Index ranges	-31 ≤ h ≤ 31, -8 ≤ k ≤ 7, -16 ≤ l ≤ 16	-26 ≤ h ≤ 26, -26 ≤ k ≤ 26, -13 ≤ l ≤ 13
Reflections collected	38240	12174
Independent reflections	4531 [R_{int} = 0.0214, R_{sigma} = 0.0121]	1789 [R_{int} = 0.1025, R_{sigma} = 0.0555]
Data/restraints/parameters	4531/0/199	1789/0/146
Goodness-of-fit on F^2	1.104	0.971
Final R indexes [I>=2σ (I)]	R_1 = 0.0170, wR_2 = 0.0393	R_1 = 0.0337, wR_2 = 0.0641
Final R indexes [all data]	R_1 = 0.0192, wR_2 = 0.0405	R_1 = 0.0468, wR_2 = 0.0663
Largest diff. peak/hole / e Å^{-3}	0.62/-0.70	0.61/-1.78
Diffractometer	Bruker APEX-II CCD	STOE IPDS 2T
CCDC access code	2250207	2244435

Table S1(continued): Crystallographic data and data collection parameters

	$HCF_3pyTeBr_2]$ (**3**)	$[ReO_2Cl(pyTeCl)(PPh_3)_2]$ (**5**)
Empirical formula	$C_{12}H_8Br_4F_6N_2Te_2$	$C_{41}H_{34}Cl_2NO_2ReTeP_2$
Formula weight	869.04	1019.33
Temperature/K	293(2)	100(2)
Crystal system	monoclinic	Triclinic
Space group	C2/c	P-1
a/Å	25.199(5)	9.075(3)
b/Å	14.306(3)	10.843(2)
c/Å	9.130(2)	19.747(5)
α/°	90	89.909(7)
β/°	100.12(3)	88.339(8)
γ/°	90	76.995(8)
Volume/Å^3	3239.9(3)	1892.6(8)
Z	6	2
ρ_{calc}g / cm^3	2.672	1.789
μ / mm^{-1}	10.151	4.228
F(000)	2352.0	988.0
Crystal size / mm^3	0.35 x 0.30 × 0.20	015 × 0.08 × 0.03
Radiation	MoKα (λ = 0.71073)	MoKα (λ = 0.71073)
2Θ range for data collection/°	9.682 to 58.71	4.608 to 54.41
Index ranges	-23 ≤ h ≤ 34, -19 ≤ k ≤ 19, -12 ≤ l ≤ 12	-11 ≤ h ≤ 11, -13 ≤ k ≤ 12, -25 ≤ l ≤ 25
Reflections collected	10616	28044
Independent reflections	4315 [R_{int} = 0.0669, R_{sigma} = 0.0664]	8352 [R_{int} = 0.0343, R_{sigma} = 0.0345]
Data/restraints/parameters	4315/293/182	8352/0/451
Goodness-of-fit on F^2	1.015	1.055
Final R indexes [I>=2σ (I)]	R_1 = 0.0547, wR_2 = 0.1191	R_1 = 0.0229, wR_2 = 0.0502
Final R indexes [all data]	R_1 = 0.0960, wR_2 = 0.1330	R_1 = 0.0266, wR_2 = 0.0514
Largest diff. peak/hole / e Å^{-3}	1.10/-1.27	1.03/-1.52
Diffractometer	STOE IPDS 2T	Bruker APEX-II CCD
CCDC access code	2244436	2244437

Table S1 (continued): Crystallographic data and data collection parameters

	$[ReO_2Cl(CF_3pyTeCl)(PPh_3)_2]$ x 3 DMF (**4**) x 3 DMF
Empirical formula	$C_{51}H_{54}Cl_2F_3N_4O_5P_2ReTe$
Formula weight	1306.62
Temperature/K	293(2)
Crystal system	triclinic
Space group	P-1
a/Å	11.0562(6)
b/Å	16.6692(8)
c/Å	16.8624(9)
α/°	66.061(4)
β/°	72.958(4)
γ/°	76.854(4)
Volume/Å^3	2694.6(3)
Z	2
ρ_{calc}g / cm^3	1.610
μ / mm^{-1}	3.002
F(000)	1292.0
Crystal size / mm^3	0.40 x 0.35 × 0.31
Radiation	MoKα (λ = 0.71073)
2Θ range for data collection/°	3.884 to 49.998
Index ranges	-13 ≤ h ≤ 13, -19 ≤ k ≤ 19, -19 ≤ l ≤ 20
Reflections collected	21118
Independent reflections	9430 [R_{int} = 0.0756, R_{sigma} = 0.0890]
Data/restraints/parameters	9430/0/628
Goodness-of-fit on F^2	0.890
Final R indexes [I>=2σ (I)]	R_1 = 0.0335, wR_2 = 0.0580
Final R indexes [all data]	R_1 = 0.0586, wR_2 = 0.0669
Largest diff. peak/hole / e Å^{-3}	1.36/--0.93
Diffractometer	STOE IPDS 2T
CCDC access code	2244438

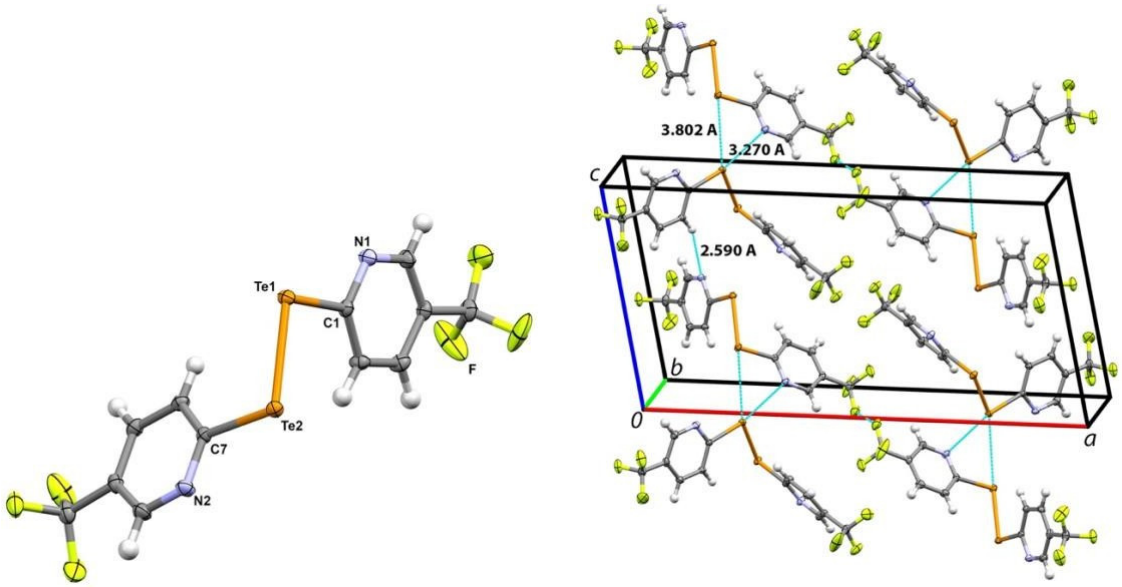

Figure S1. Structure of $(CF_3pyTe)_2$ (**1**). Ellipsoid plot with thermal ellipsoids representing 50 per cent probability and unit cell plot illustrating secondary Te…Te bonds of 3.802 Å, intermolecular Te…N contacts of 3.270 Å and a weak intermolecular H bond of 2.590 Å.

Table S2. Selected bond lengths (Å) and angles (°) in $(CF_3pyTe)_2$ (**1**).

Te1-Te2	2.689(2)	Te1-C1	2.139(2)	Te2-C7	2.132(2)
C1-Te1-Te2	99.83(6)	C7-Te2-Te1	100.05(6)		

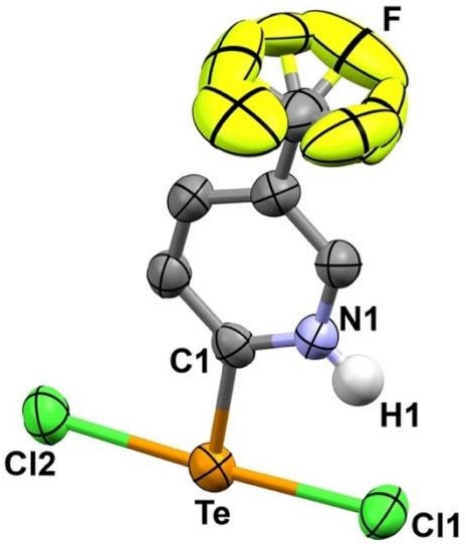

Figure S2. Ellipsoid representation of the molecular structure of $(HCF_3py)TeCl_2$ (**2**). Thermal ellipsoids represent 50 per cent probability.

Table S3. Selected bond lengths (Å) and angles (°) in $(HCF_3py)TeCl_2$ (**2**).

Te-Cl1	2.576(1)	Te-Cl2	2.525(1)	Te-C1	2.120(5)
Cl1-Te-Cl2	177.29(5)	Cl1-Te-C1	87.1(1)	Cl2-Te1-C1	90.4(1)

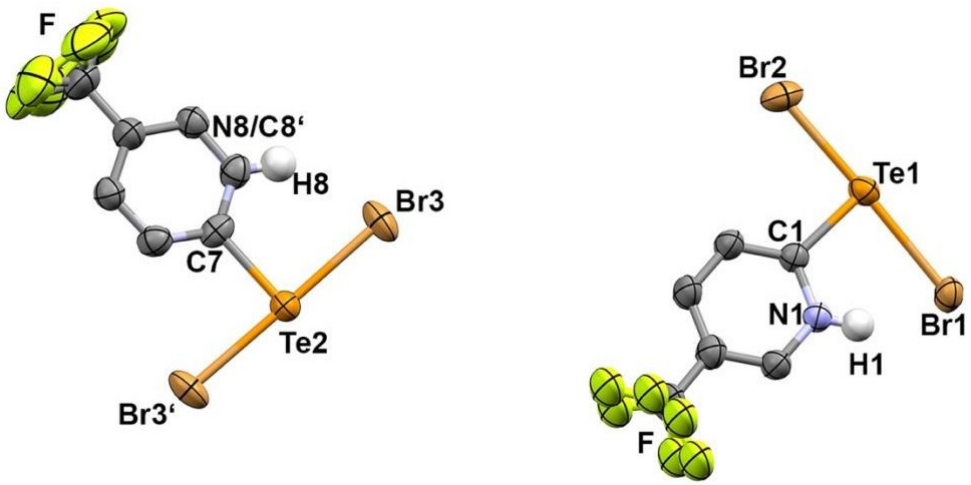

Figure S3. Ellipsoid representation of the molecular structure of (HCF_3py)$TeBr_2$ (**3**). Thermal ellipsoids represent 50 per cent probability.

Table S4. Selected bond lengths (Å) and angles (°) in (HCF_3py)$TeBr_2$ (**3**).

Te1-Br1	2.819(1)	Te1-Br2	2.640(1)	Te1-C1	2.123(3)
Te2-Br3	2.706(1)	Te2-C7	2.15(1)		
Br1-Te1-Br2	178.24(4)	Br1-Te1-C1	87.6(1)	Br2-Te1-C1	90.7(1)
Br3-Te2-Br3’	179.13(6)	Br3-Te2-C7	89.56(3)		

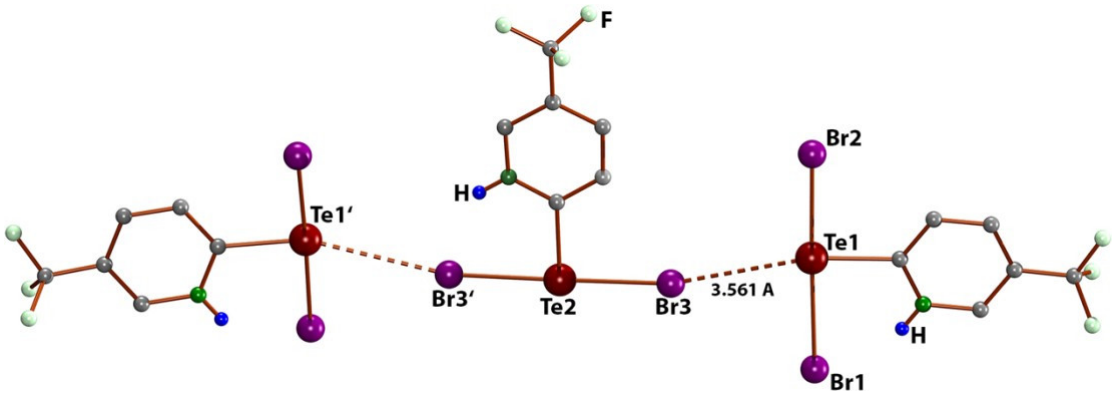

Figure S4. ‘Long-range’ Te-Br interactions in (HCF_3py)$TeBr_2$ (**3**).

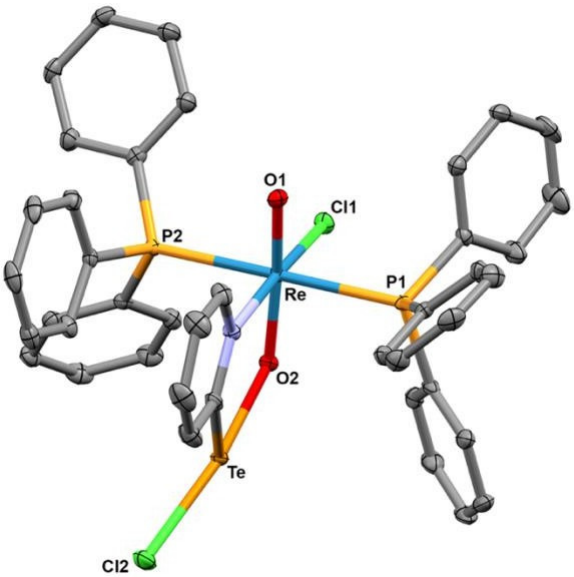

Figure S5. Ellipsoid representation of the molecular structure of $[ReO_2Cl(pyTeCl)(PPh_3)_2]$ (**5**). Thermal ellipsoids represent 50 per cent probability.

Table S5. Selected bond lengths (Å) and angles (°) in $[ReO_2Cl(pyTeCl)(PPh_3)_2]$ (**5**).

Re-O1	1.730(2)	Re-O2	1.824(2)	Re-N1	2.193(2)
Re-Cl1	2.3816(8)	Re-P1	2.5192(9)	Re-P2	2.5012(9)
O2-Te	2.102(2)	Te-Cl2	2.5736(9)	Te-C1	2.136(3)
O1-Re-O2	168.42(9)	O1-Re-N1	87.80(9)	O1-Re-Cl1	97.87(7)
O1-Re-P1	91.46(7)	O1-Re-P2	90.52(7)	Re-O2-Te	134.3(1)
O2-Te-C1	81.23(9)	Re-N1-C1	134.7(2)	N1-C1-Te	117.8(2)

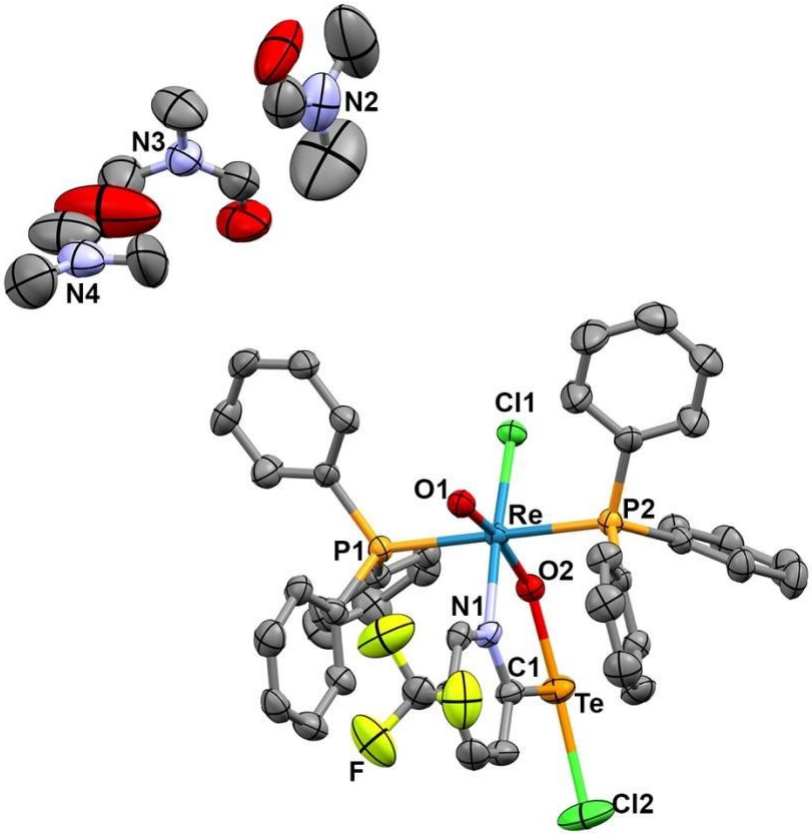

Figure S6. Ellipsoid representation of the molecular structure of $[ReO_2Cl(CF_3pyTeCl)(PPh_3)_2]$ (**4**) x 3 DMF. Thermal ellipsoids represent 50 per cent probability.

Table S6. Selected bond lengths (Å) and angles (°) in $[ReO_2Cl(CF_3pyTeCl)(PPh_3)_2]$ (**4**).

Re-O1	1.721(4)	Re-O2	1.822(3)	Re-N1	2.201(4)
Re-Cl1	2.383(1)	Re-P1	2.511(1)	Re-P2	2.514(1)
O2-Te	2.102(4)	Te-Cl2	2.578(2)	Te-C1	2.125(5)
O1-Re-O2	165.9(2)	O1-Re-N1	86.2(2)	O1-Re-Cl1	99.7(1)
O1-Re-P1	88.3(1)	O1-Re-P2	89.3(2)	Re-O2-Te	135.2(2)
O2-Te-C1	81.0(2)	Re-N1-C1	125.2(3)	N1-C1-Te	118.3(4)

2. Spectroscopic Data

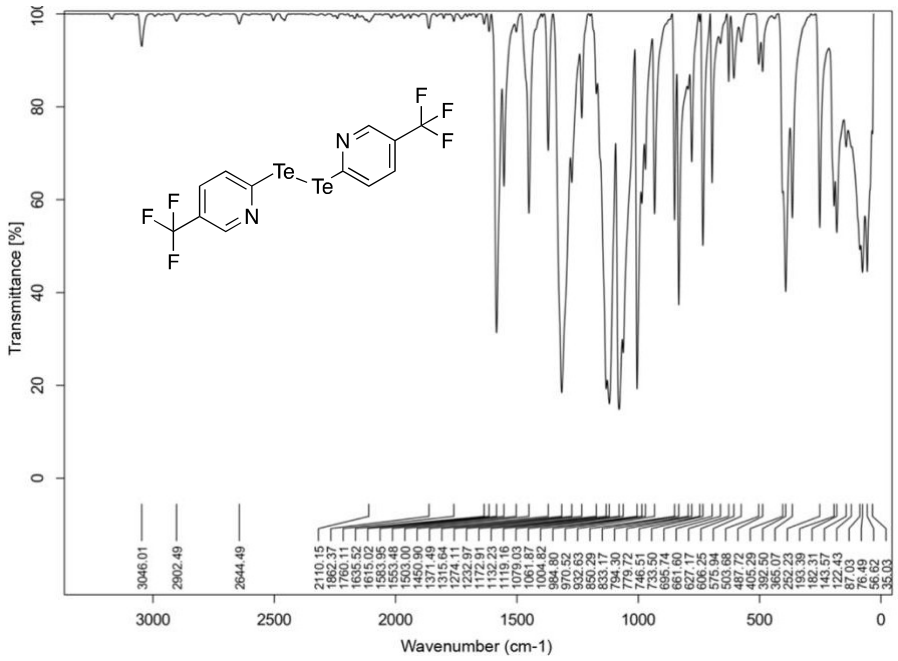

Figure S7. IR spectrum of bis(5-trifluoromethyl-2-pyridyl)ditellane (**1**)

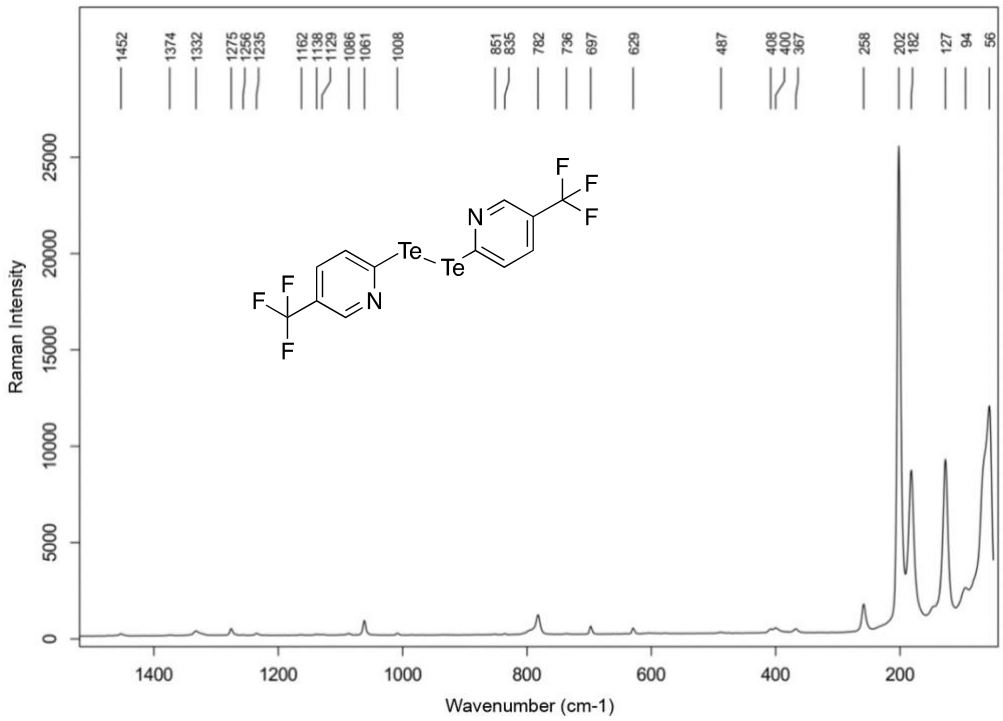

Figure S8. Raman spectrum of bis(5-trifluoromethyl-2-pyridyl)ditellane (**1**)

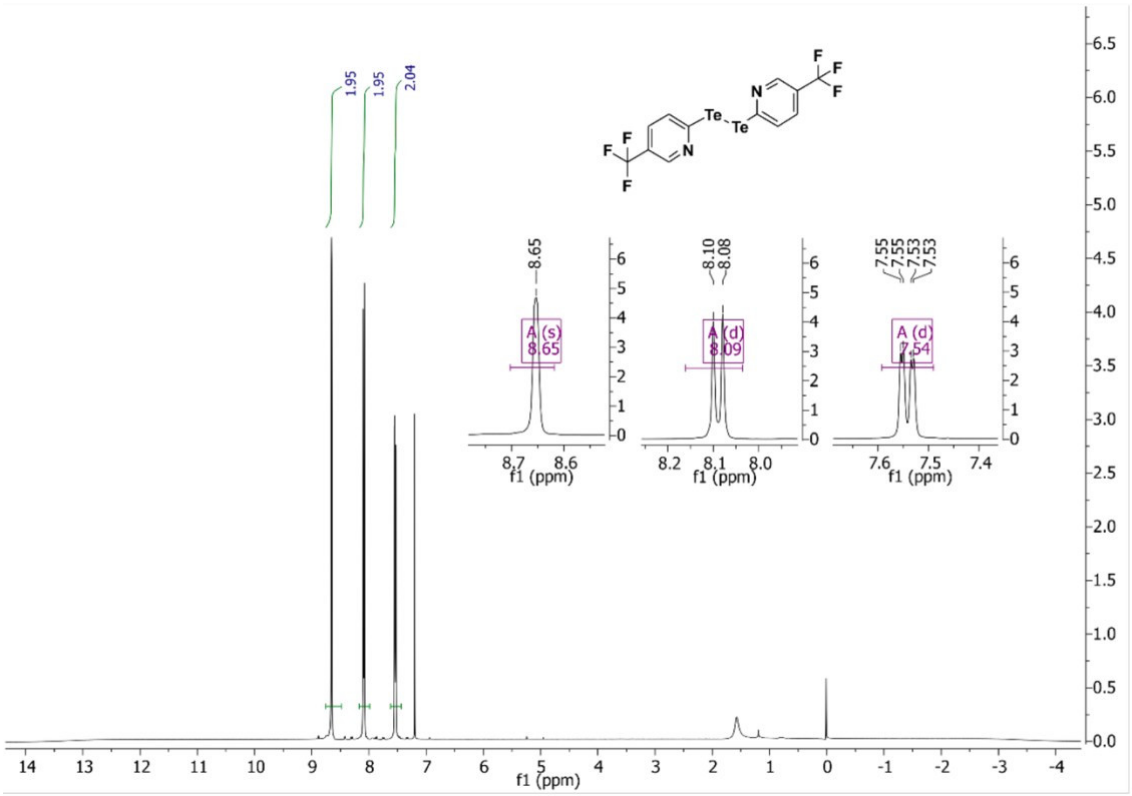

Figure S9. ^{1}H NMR spectrum of bis(5-trifluoromethyl-2-pyridyl)ditellane (**1**) in $CDCl_3$.

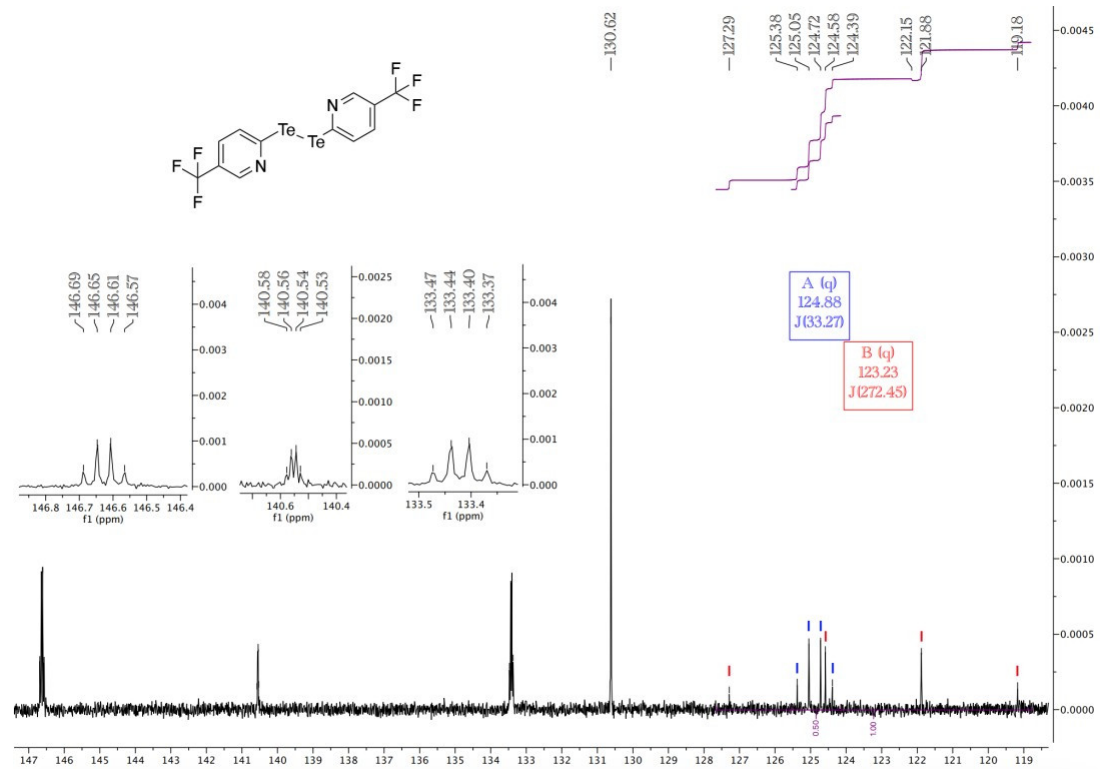

Figure S10. ^{13}C NMR spectrum of bis(5-trifluoromethyl-2-pyridyl)ditellane (**1**) in $CDCl_3$.

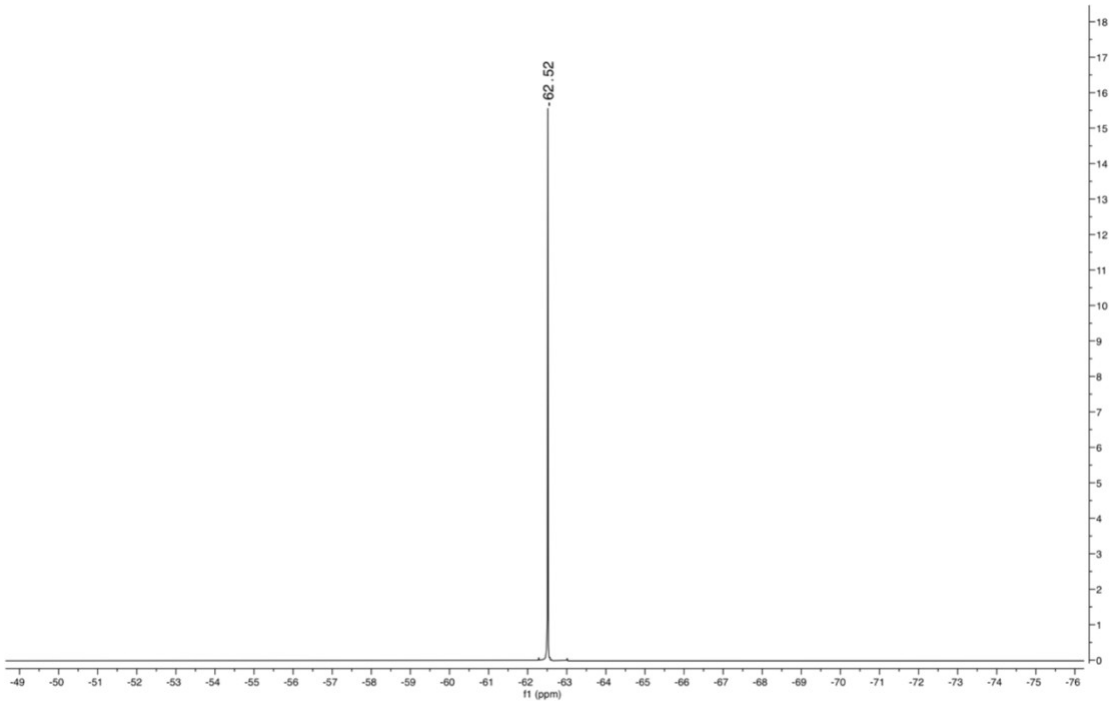

Figure S11. ^{19}F NMR spectrum of bis(5-trifluoromethyl-2-pyridyl)ditellane (**1**) in $CDCl_3$.

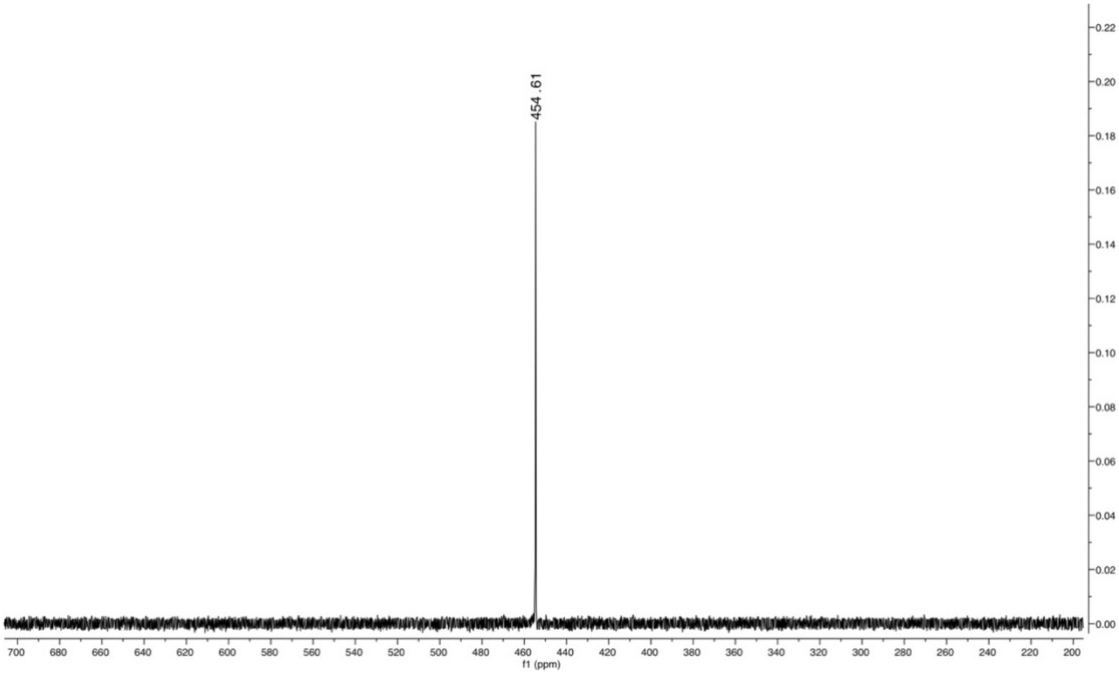

Figure S12. ^{125}Te NMR spectrum of bis(5-trifluoromethyl-2-pyridyl)ditellane (**1**) in $CDCl_3$.

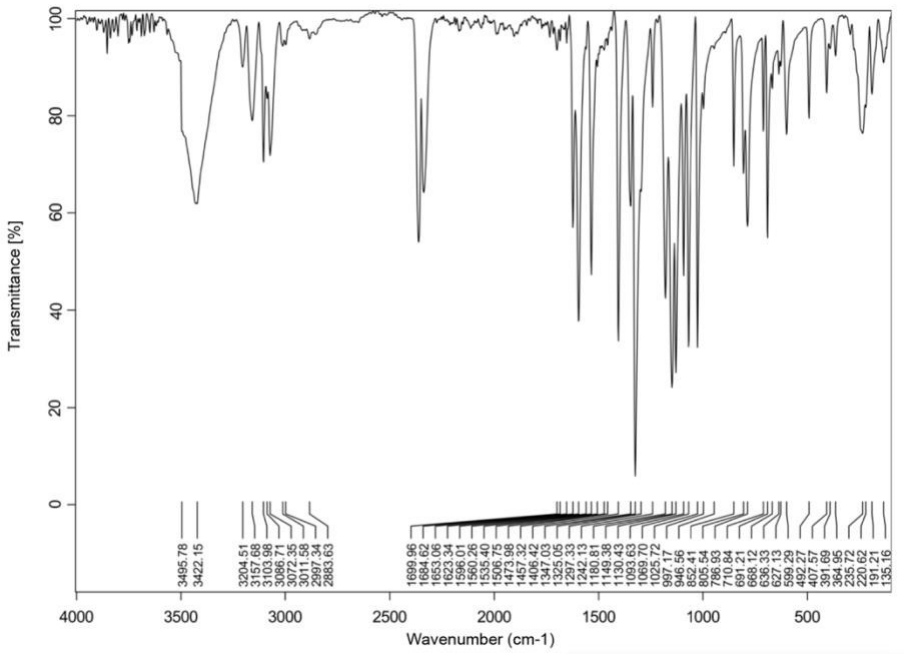

Figure S13. IR spectrum of $(HCF_3py)TeCl_2$ (**2**).

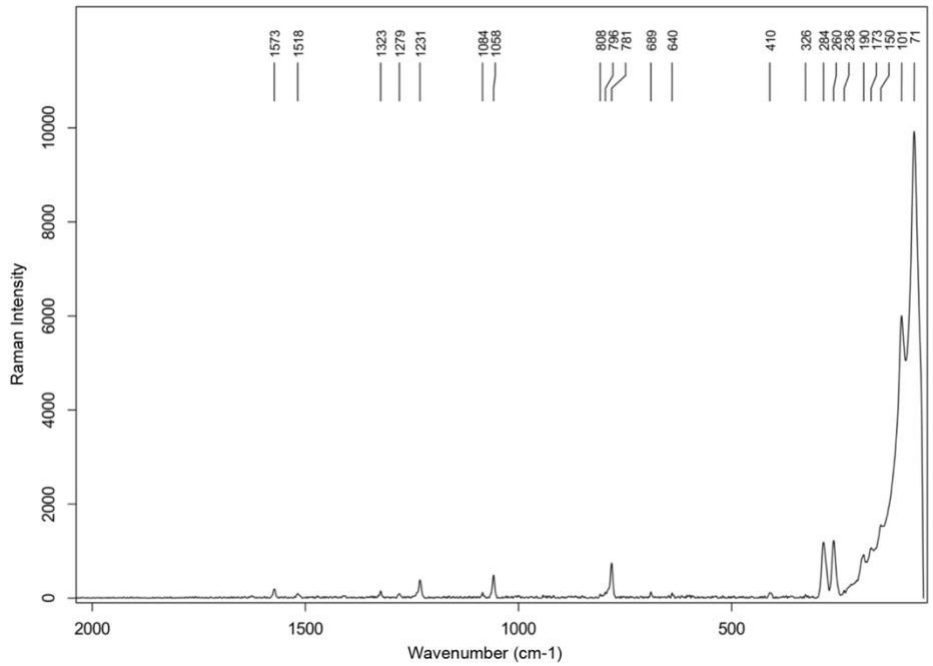

Figure S14. Raman spectrum of $(CF_3pyH)TeCl_2$ (**2**).

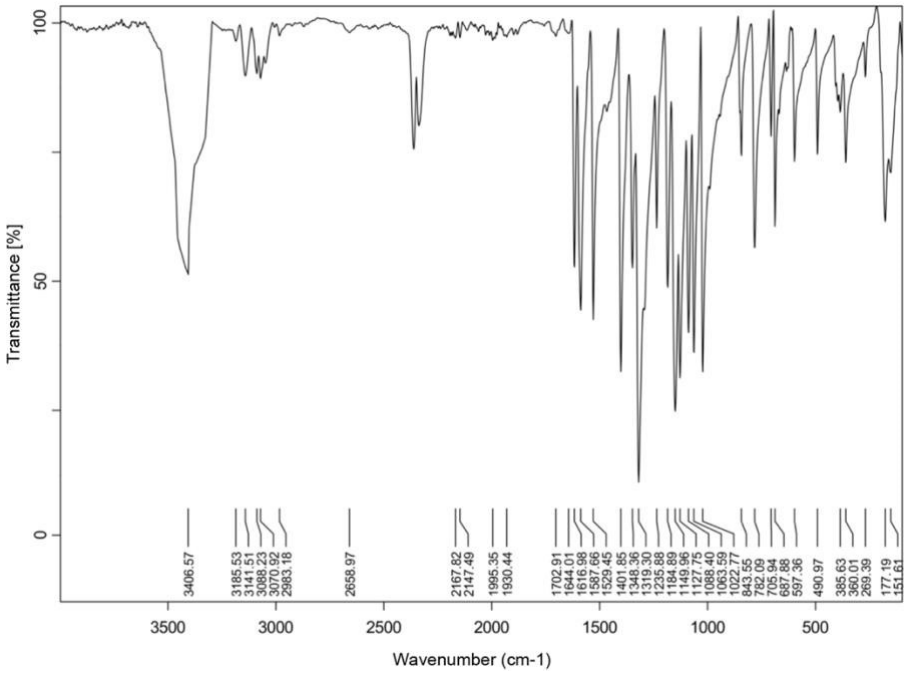

Figure S15. IR spectrum of $(HCF_3py)TeBr_2$ (**3**).

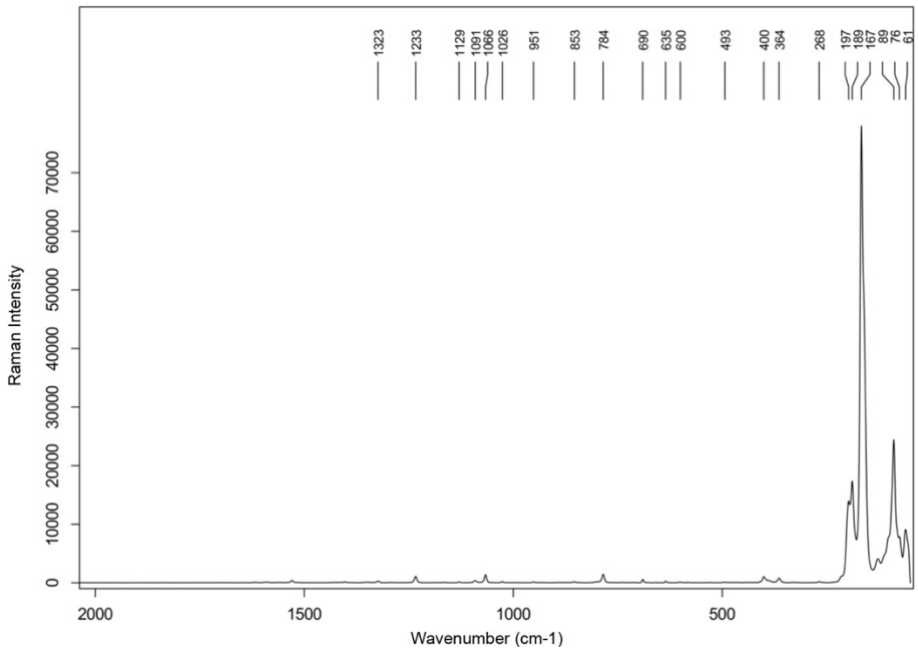

Figure S16. Raman spectrum of $(HCF_3py)TeBr_2$ (**3**).

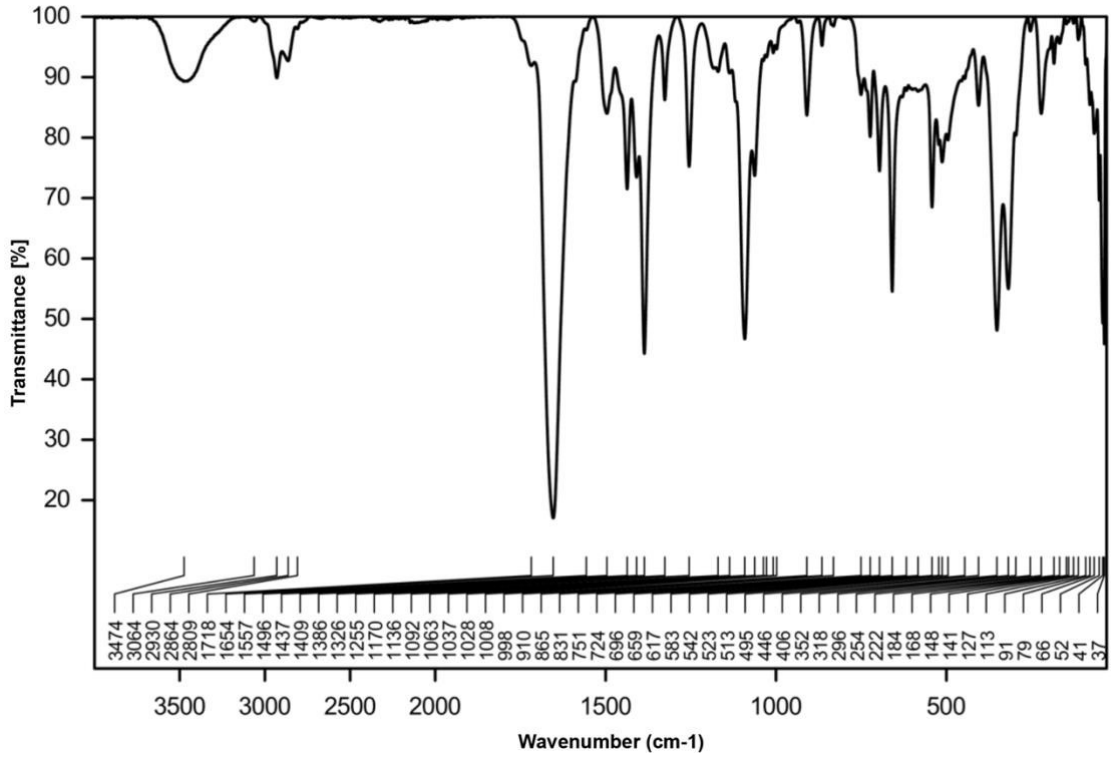

Figure S17. IR spectrum of $[ReO_2Cl(CF_3pyTeCl)(PPh_3)_2]$ (**4**).

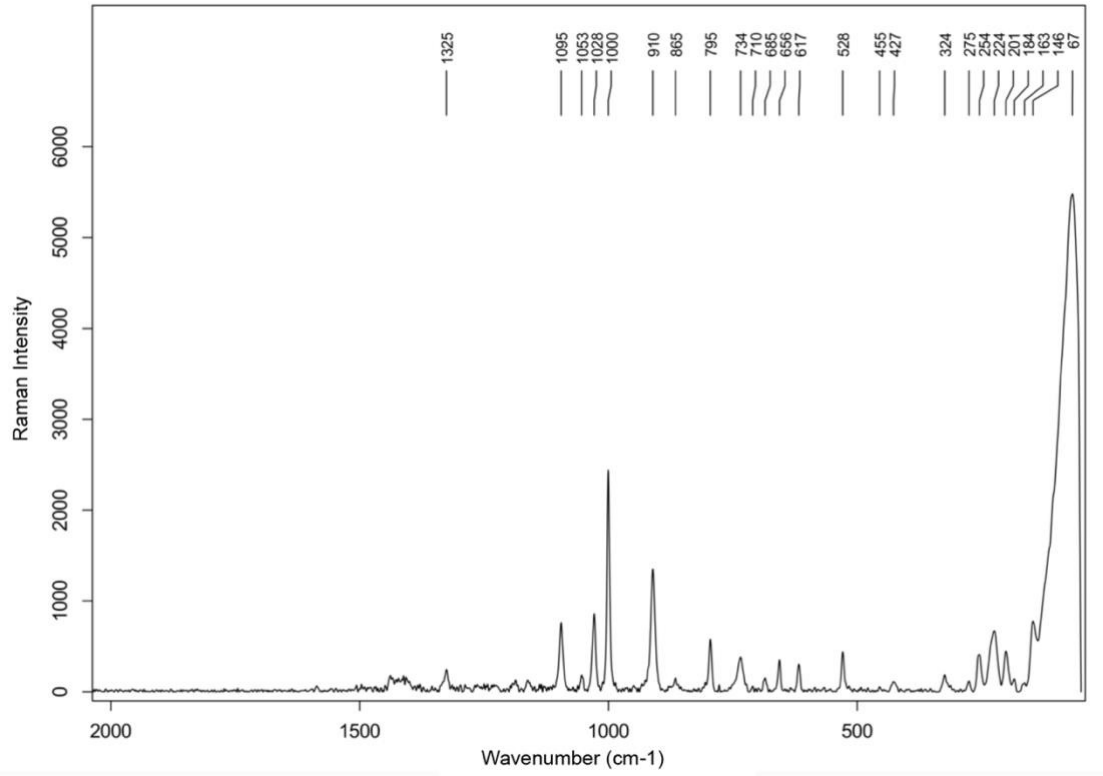

Figure S18. Raman spectrum of $[ReO_2Cl(CF_3pyTeCl)(PPh_3)_2]$ (**4**)

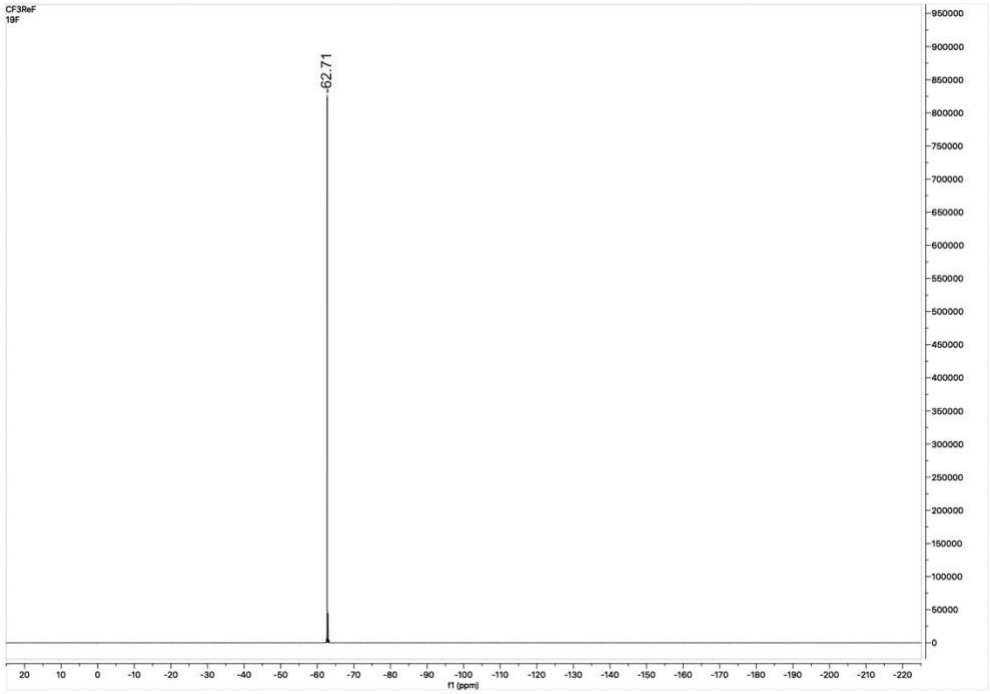

Figure S19. ^{19}F NMR spectrum of $[ReO_2Cl(CF_3pyTeCl)(PPh_3)_2]$ (**4**).

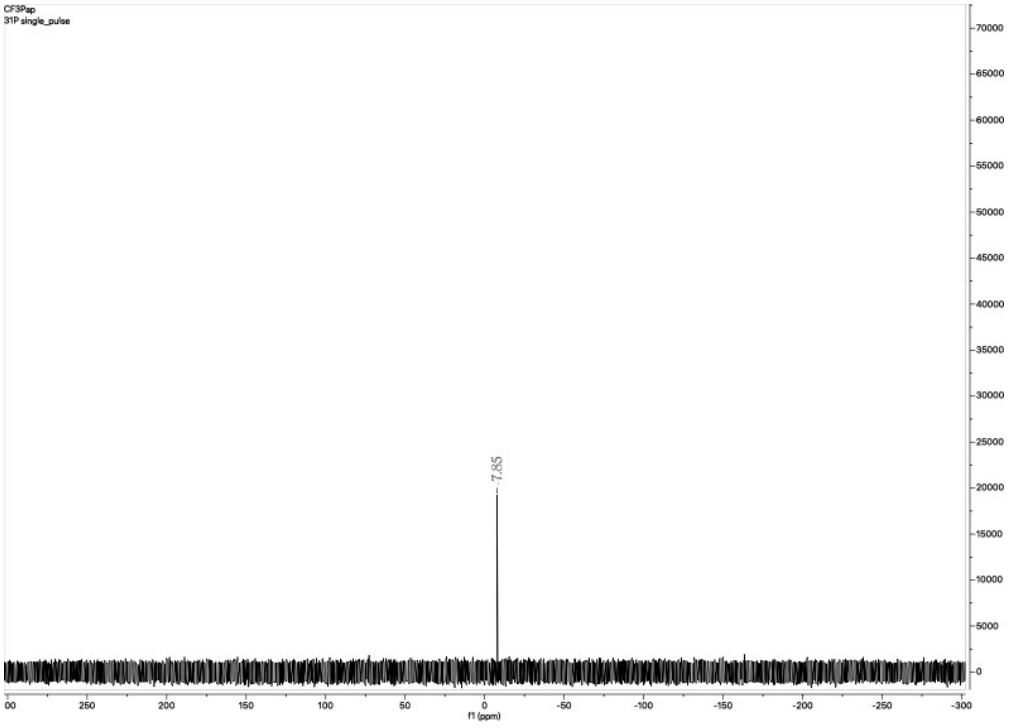

Figure S20. ^{31}P NMR spectrum of $[ReO_2Cl(CF_3pyTeCl)(PPh_3)_2]$ (**4**).

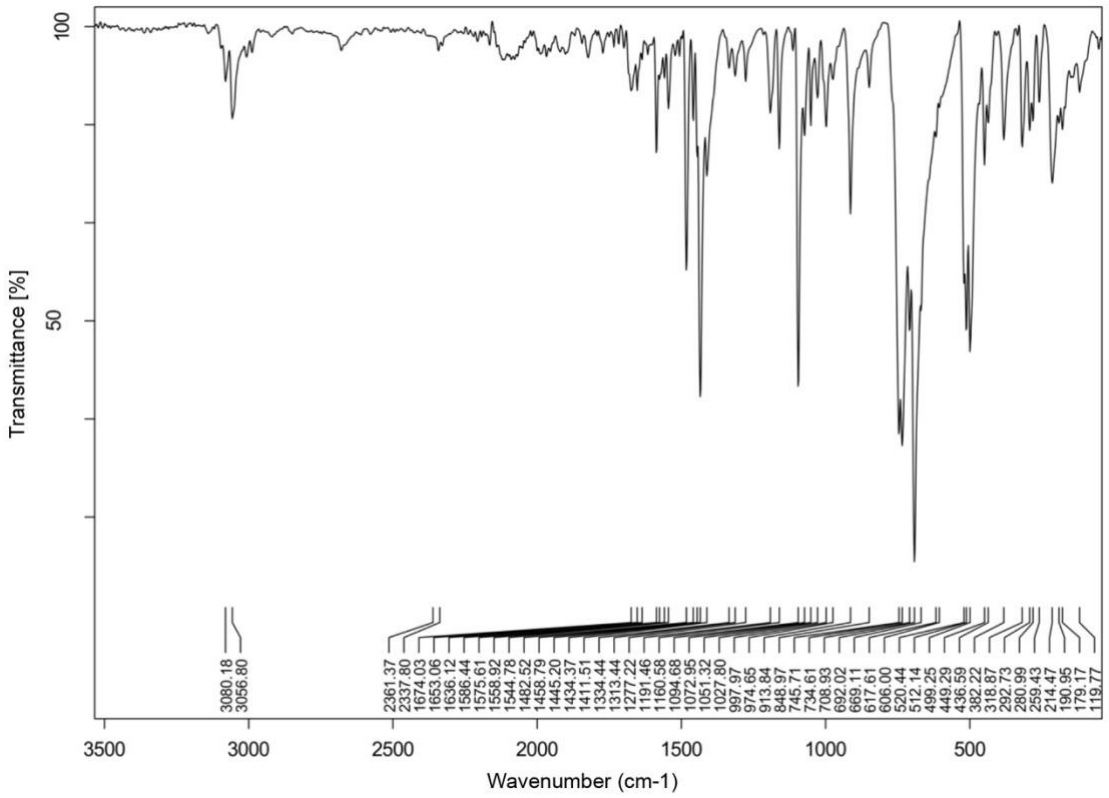

Figure S21. IR spectrum of $[ReO_2Cl(pyTeCl)(PPh_3)_2]$ (**5**).

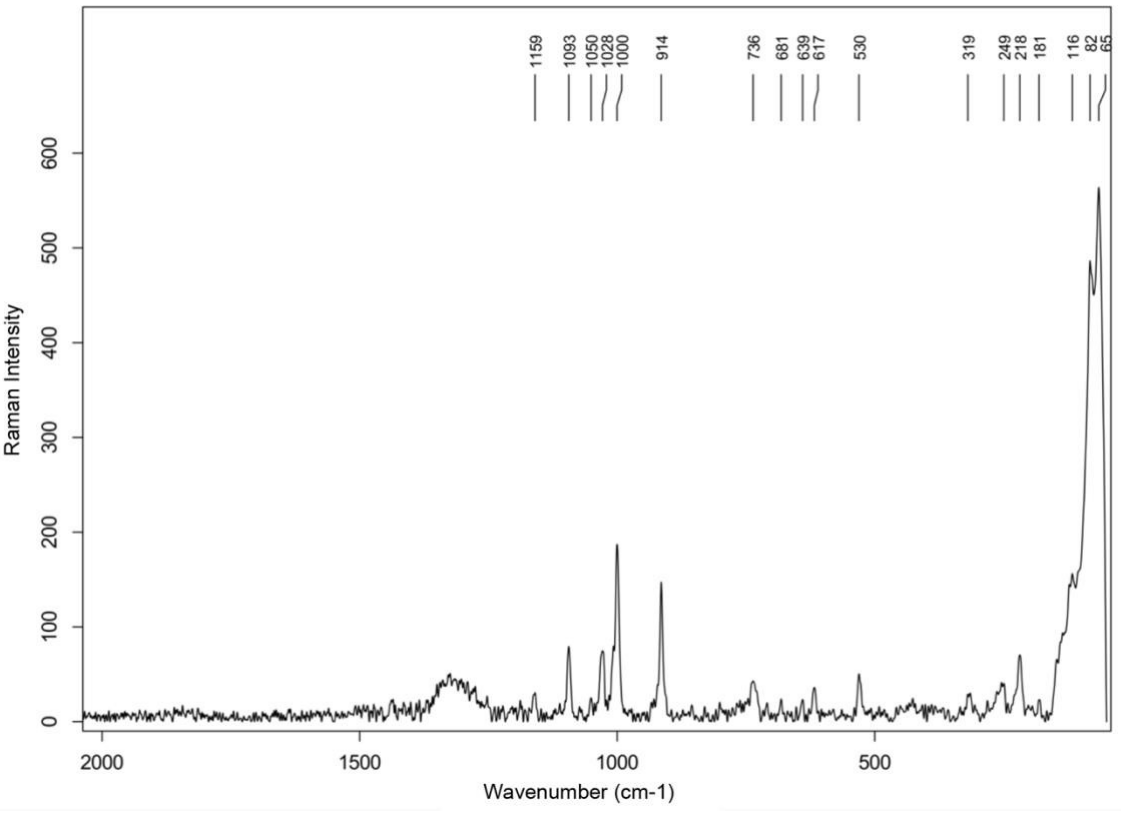

Figure S22. Raman spectrum of $[ReO_2Cl(pyTeCl)(PPh_3)_2]$ (**5**).

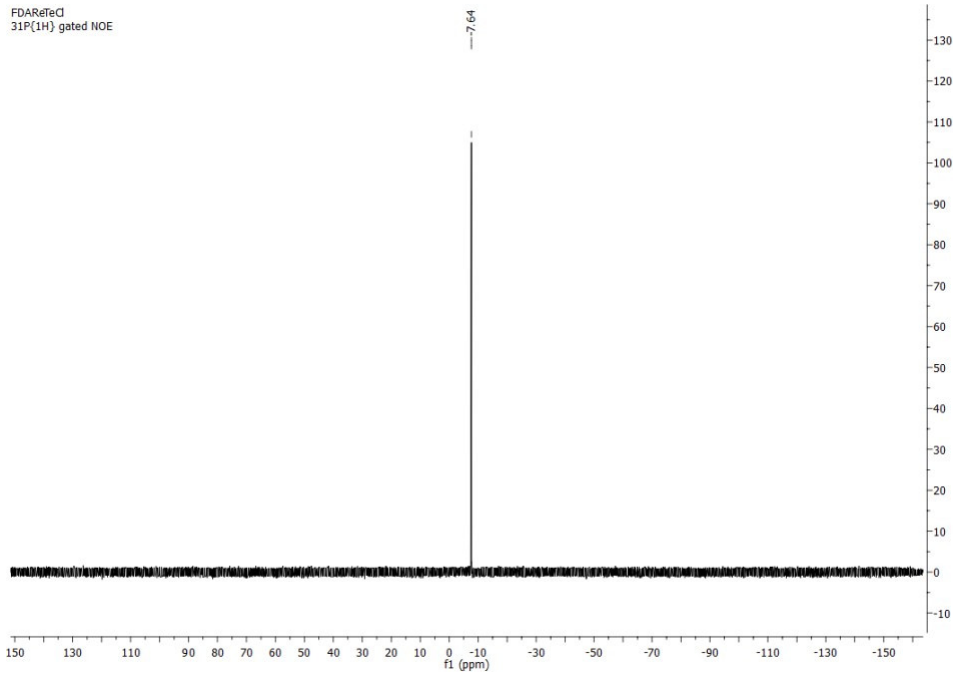

Figure S23. ^{31}P NMR spectrum of $[ReO_2Cl(pyTeCl)(PPh_3)_2]$ (**5**).

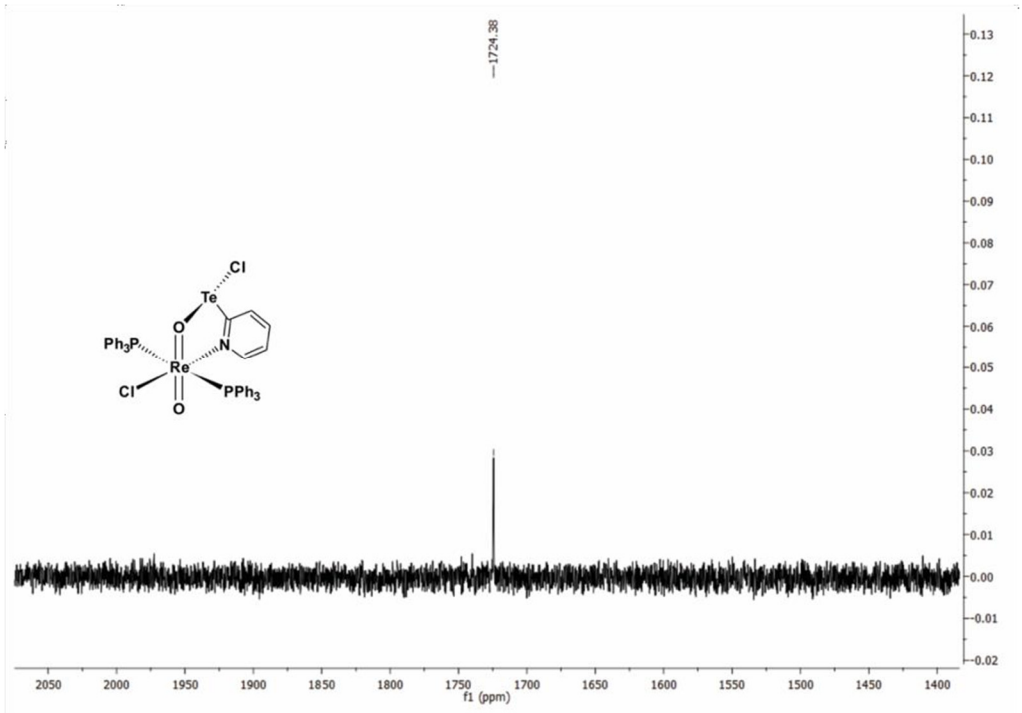

Figure S24. ^{125}Te NMR spectrum of $[ReO_2Cl(pyTeCl)(PPh_3)_2]$ (**5**).

S3. Computational Chemistry

Table S7. Results of the charge analysis for selected atoms in $[ReO_2Cl(pyTeCl)(PPh_3)_2]$ (**5**). Wiberg bond order matrix for selected atoms, relevant bond orders are bold.

	Bader charge	**ADCH charge**	**Wiberg bond order matrix**							
			Re1	Te2	O5	Cl4	N6	Cl11	O12	C75
Re1	2.963592	1.664582	**6.6**	0.1	**0.8**	0	**0.4**	**1.0**	**2.2**	0.1
Te2	1.331715	0.811975		**2.4**	**0.7**	**0.3**	0.1	0	0	**0.9**
O5	-1.955526	-1.374591			**2.0**	0	0	0.1	0.1	0.1
Cl4	-1.020208	-0.928387				**0.4**	0	0	0	0
N6	-1.340768	-0.262371					**3.8**	0	0	**1.9**
Cl11	-0.638446	-0.467039						**1.3**	0.1	0
O12	-0.979281	-0.467644							**2.9**	0
C75	0.499392	0.334154								**4.4**

Table S8. Lone-pair decomposition of Re and Te in $[ReO_2Cl(pyTeCl)(PPh_3)_2]$ (**5**).

Orbital	Population	s	p	d
LP(1)Re	1.94282	0.00%	0.01%	99.99%
LP(1)Te	1.98754	88.25%	11.74%	0.01%
LP(2)Te	1.80730	0.00%	99.94%	0.06%

Table S9. Natural electron configuration of selected atoms in $[ReO_2Cl(pyTeCl)(PPh_3)_2]$ (**5**).

Re1	[core]6s(0.41)5d(5.60)6p(0.01)6d(0.05)7p(0.01)
Te2	[core]5s(1.84)5p(3.21)5d(0.01)6p(0.01)
Cl4	[core]3s(1.97)3p(5.61)
O5	[core]2s(1.81)2p(5.02)3p(0.01)4p(0.01)
N6	[core]2s(1.30)2p(4.18)3p(0.02)
Cl11	[core]3s(1.92)3p(5.53)
O12	[core]2s(1.84)2p(4.75)3d(0.01)

Table S10. Selected parameters from the second order perturbation analysis of $[ReO_2Cl(pyTeCl)(PPh_3)_2]$ (**5**). Delocalization, which was interpreted as an ionic bond is bold.

Donor NBO	Acceptor NBO	$E_{deloc.}$(kcal/mol)	$\Delta E_{donor\text{-}acceptor}$(a.u.)	F (a.u.)
LP(2)O1	**LV(1)Re1**	**198.08**	**0.53**	**0.289**
LP(2)Te	BD*(2)N1-C75	20.87	0.16	0.051
LP(1)Cl1	LV(1)Te	9.37	0.55	0.064
LP(4)Cl1	**LV(1)Te**	**115**	**0.19**	**0.131**
LP(1)O2	LV(1)Re	52.85	0.75	0.178
LP(2)O2	**LV(1)Re**	**95.55**	**0.41**	**0.176**
LP(2)O2	BD*(2)Re-1O1	18.23	0.26	0.062
LP(3)O2	**BD*(1)Re-1O1**	**67.66**	**0.18**	**0.1**
LP(4)O2	**LV(1)Re**	**88.04**	**0.49**	**0.186**
LP(4)O5	BD*(2)Re-1O12	11.89	0.35	0.058
LP(2)O5	**LV(1)Te2**	**68.78**	**0.23**	**0.113**
LP(1)O5	LV(1)Te2	38.46	0.58	0.133
LP(4)O5	LV(1)Te2	35.25	0.32	0.095
LP(2)Te2	BD*(2)N6-C75	20.87	0.16	0.051

Table S11. Three-centered *trans*-bonds around Re (3c4e hyper-bonds) in $[ReO_2Cl(pyTeCl)(PPh_3)_2]$ (**5**).

Hyperbond	A:-B-:C	%A-B/%B-C	occ	BD(A-B)	LP(C)	h(A)	h(B)	h(C)
1	P1:-Re-:P2	49.5/50.5	3.9456	67	61	67	68	61
2	Cl1:-Re-:N	57.1/42.9	4.0453	68	60	69	70	60
3	O1:-Re-:O2	57.4/42.6	4.0369	69	58	71	72	58

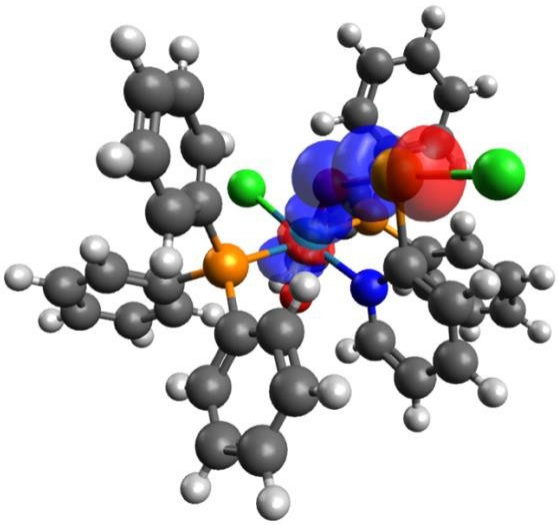

Figure S25. Donation of lone pair 1 (LP1) of O2 into empty valence orbital 1 (LV1) of Re and Te in $[ReO_2Cl(pyTeCl)(PPh_3)_2]$ (**5**) based on the NBO analysis. The isosurfaces are shown with an isosurface value of 0.08.

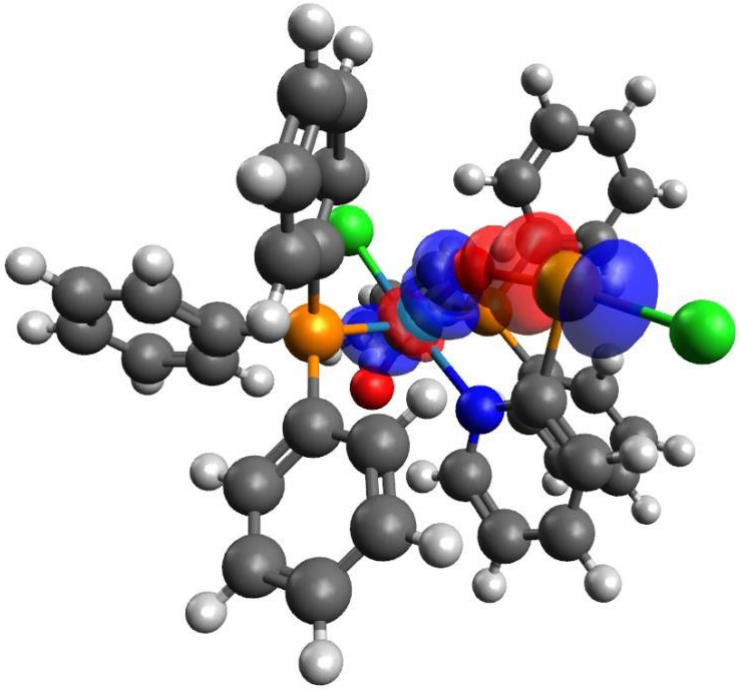

Figure S26.. Donation of lone pair 2 (LP2) of O2 into empty valence orbital 1 (LV1) of Re and Te in $[ReO_2Cl(pyTeCl)(PPh_3)_2]$ (**5**) based on the NBO analysis. The isosurfaces are shown with an isosurface value of 0.08.

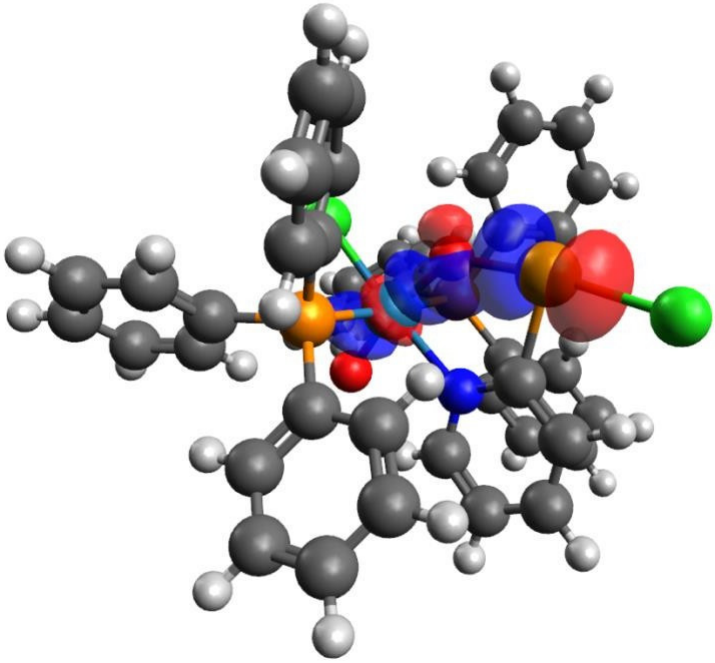

Figure S27. Donation of lone pair 4 (LP4) of O2 into empty valence orbital 1 (LV1) of Re and Te in $[ReO_2Cl(pyTeCl)(PPh_3)_2]$ (**5**) based on the NBO analysis. The isosurfaces are shown with an isosurface value of 0.08.

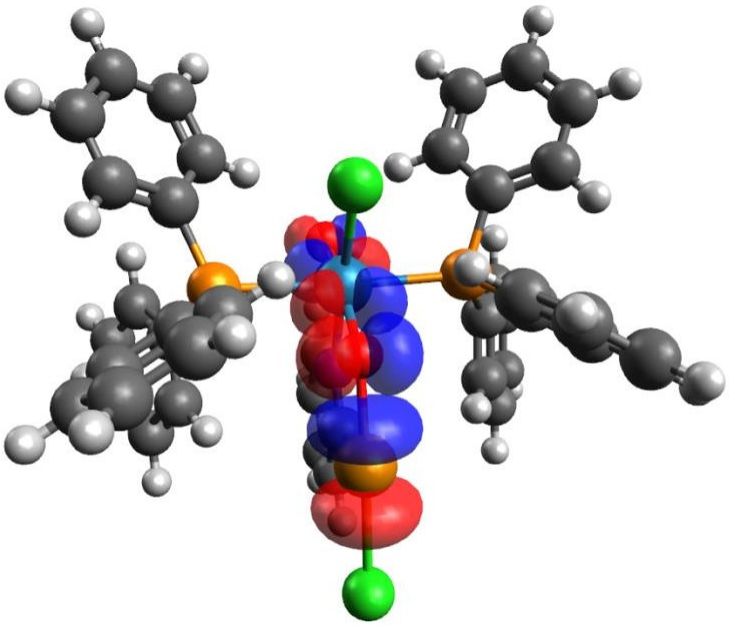

Figure S28. Donation of lone pair 3 (LP3) of O2 into the antibonding Re-O1 orbital of $[ReO_2Cl(pyTeCl)(PPh_3)_2]$ (**5**) based on the NBO analysis. LV1 of Te is also shown to visualize the orthogonality of the two orbitals and the absence of donation of LP3 of O2 into this orbital. The isosurfaces are shown with an isosurface value of 0.08.

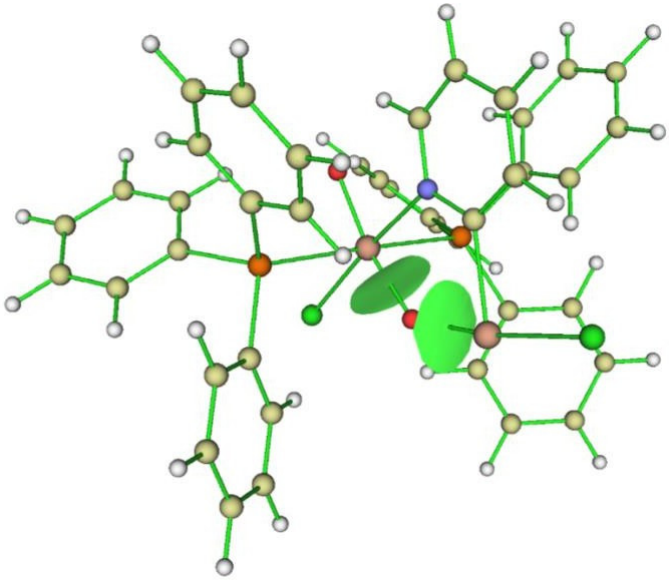

Figure S29. Interbasin surfaces of Re-O2 and Te-O2 contacts in $[ReO_2Cl(pyTeCl)(PPh_3)_2]$ (**5**).

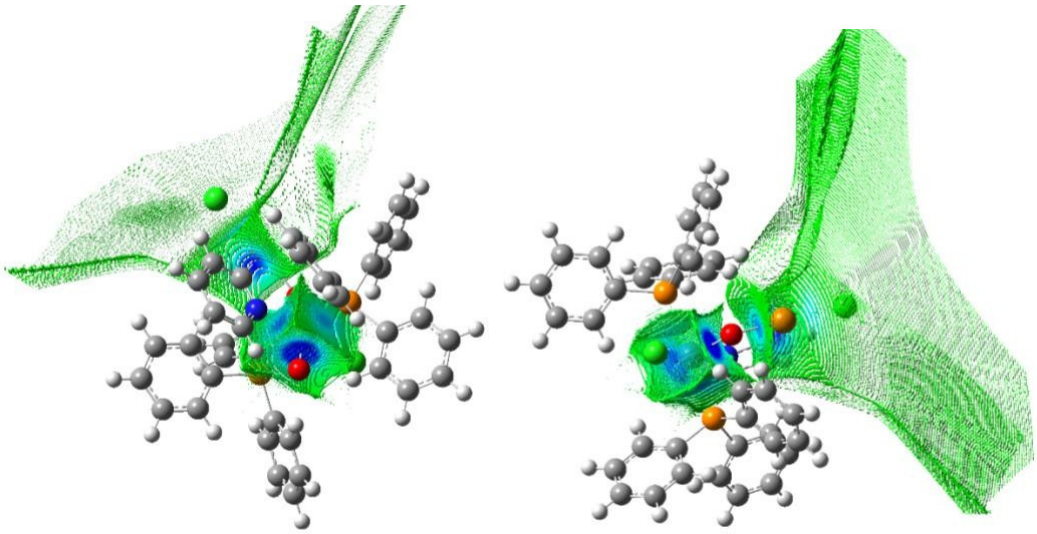

Figure S30. Basins of Re and Te in $[ReO_2Cl(pyTeCl)(PPh_3)_2]$ (**5**) with mapping of the electron density at the 0.06 isosurface value. The electron density at the surface is a measure of the bond strength.

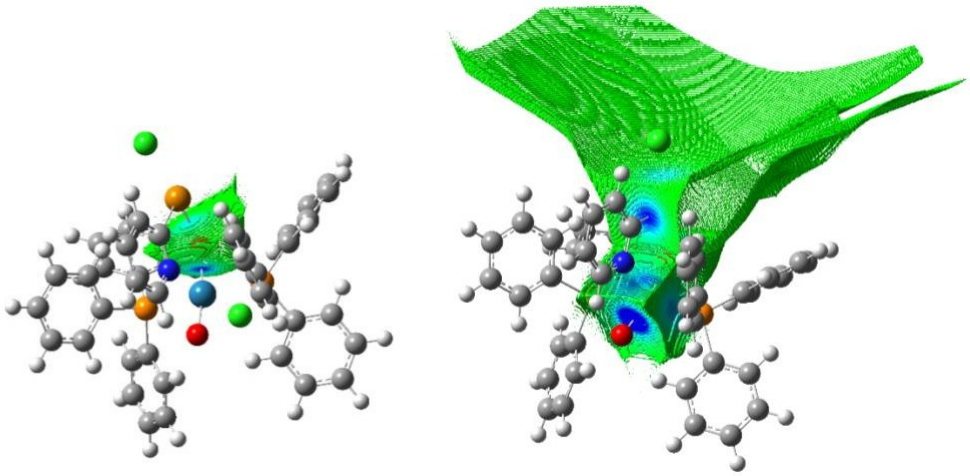

Figure S31. Basins of O2 and the superposition of Re, Te and O2 basins in $[ReO_2Cl(pyTeCl)(PPh_3)_2]$ (**5**) with mapping of the electron density at the 0.06 isosurface value. The electron density at the surface is a measure of the bond strength.

Table S12. Selected properties of the electron density at important bond critical points in $[ReO_2Cl(pyTeCl)(PPh_3)_2]$ (**5**).

(3,-1)cp	ρ(r)	$\nabla^2\rho$(r)	ε(r)	λ1(r)	λ2(r)	λ3(r)	η(r)	H(r)	$\delta(A,B)$
O1-Re	0.1753	1.3876	0.4920	-0.2226	-0.3322	1.9424	0.1710	-0.0630	1.6045
O2-Re	0.1089	1.4504	0.0371	-0.1762	1.7964	-0.1699	0.0981	-0.0028	0.3645
O2-Te	0.0507	0.4580	0.2543	-0.0456	0.5608	-0.0572	0.1020	-0.0060	0.3209

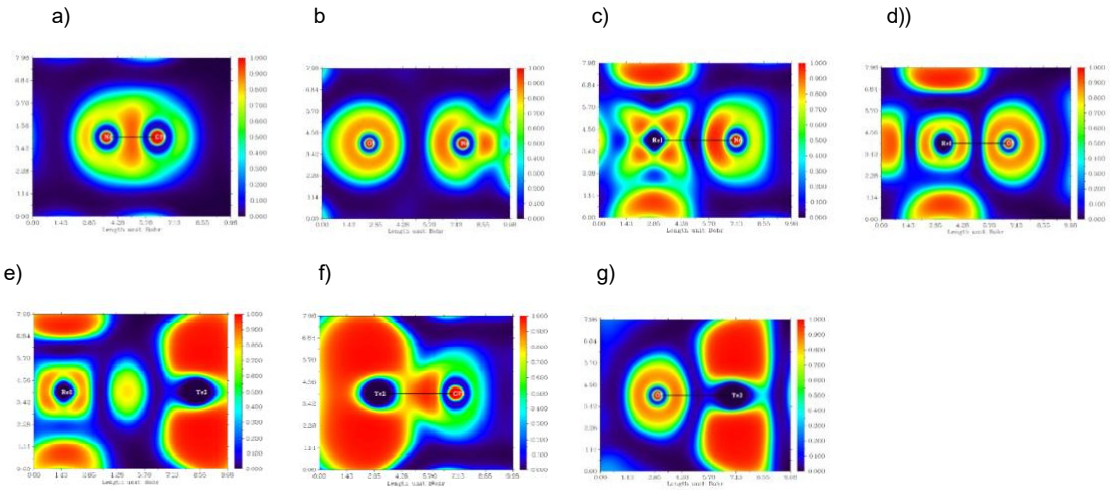

Figure S32. ELF with bond paths (black) in [$ReO_2Cl(pyTeCl)(PPh_3)_2$] (**5**). Cuts through a) the C=N bond in z direction to the pyridine plane, b) the O N contact in z direction to the pyridine plane, c) the Re-N dative bond in z direction to the pyridine plane, c) the Re-O bond in z direction to the pyridine plane or along the Re-P-O plane, e) the Re Te contact in z direction to the pyridine plane, f) the Te-C bond in z direction to the pyridine plane, g) the Te-O bond in z direction to the pyridine plane.

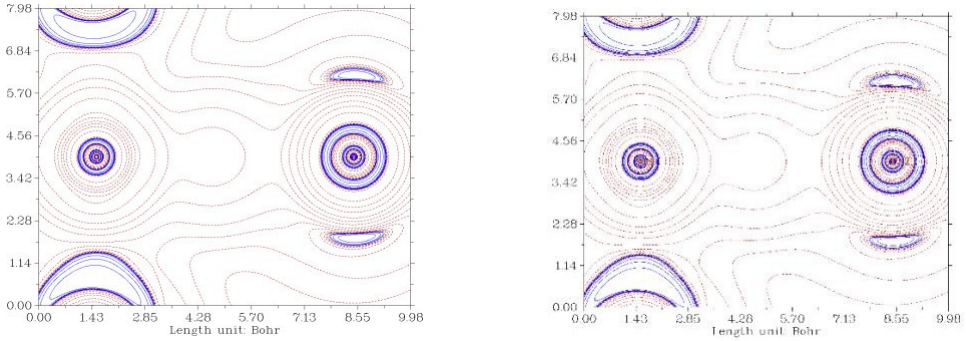

Figure S33. Laplacian map of the electron density in [$ReO_2Cl(pyTeCl)(PPh_3)_2$] (**5**) (blue = negative; red = positive) with negative values corresponding to local electronic charge accumulation while positive values indicate regions of local electronic charge depletion. Cut through the Re Te contact in z direction to the pyridine plane.

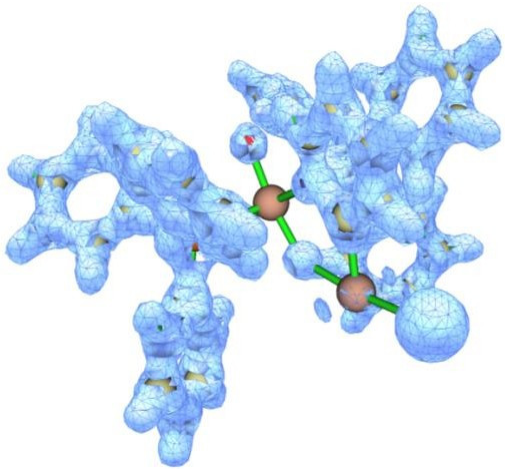

Figure S34. 3D Laplacian map of the electron density at the 0 (enclosure) level in [$ReO_2Cl(pyTeCl)(PPh_3)_2$] (**5**) showing regions of electronic charge accumulation .

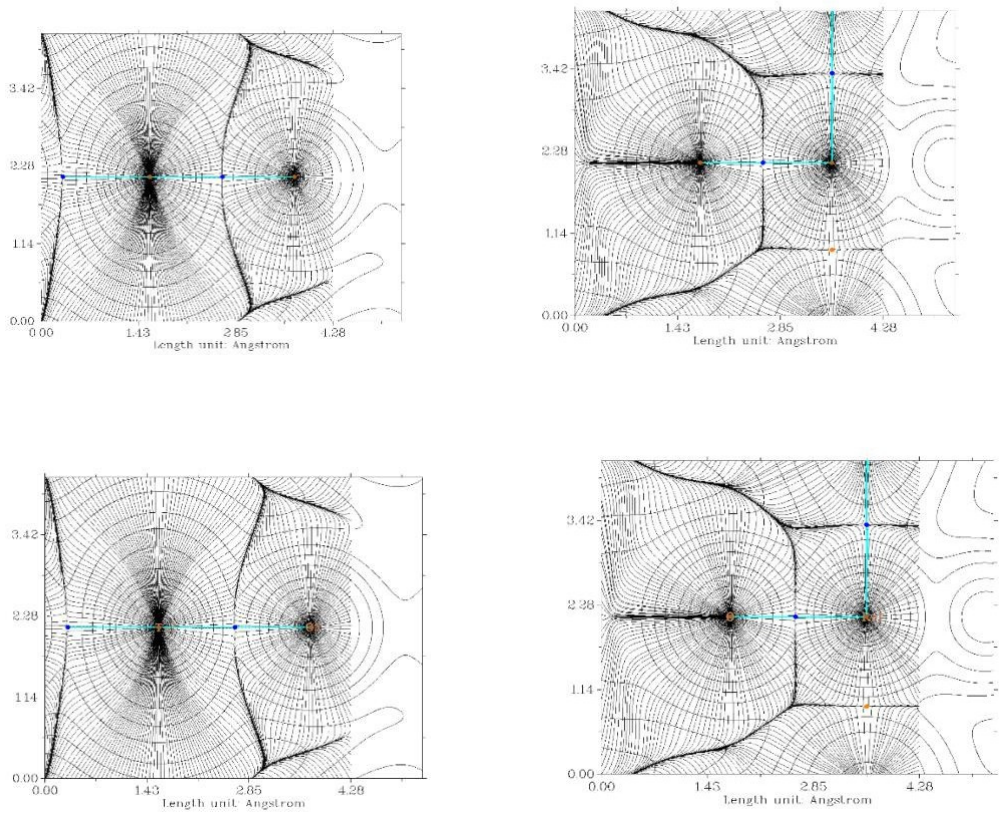

Figure S35. Gradient vector field of the electron density cut through the respective Te-O (left) and O-Re (right) bonds perpendicular to the Re-O-Te plane in [$ReO_2Cl(pyTeCl)(PPh_3)_2$] (**5**) mapped on the electron density iso contour lines with topological descriptors. (3,-3) = brown, (3,-1) = blue, (3,1) = orange, bond path between (3,-3) and (3,-1) critical points = cyan. Additionally, a contour line of the van der Waals radius (black) is shown.

S4. References

[1] Coppens, P. The Evaluation of Absorption and Extinction in Single-Crystal Structure Analysis. Crystallographic Computing; Copenhagen, Muksgaard, 1979

[2] Bruker. APEX2, SAINT and SADABS. Bruker AXS Inc., Madison, WI, USA (2009).

[3] Sheldrick, G. M.: A short history of SHELX. Acta Crystallogr.A64 (2008) 112–122.

[4] Sheldrick, G. M. Crystal structure refinement with SHELXL. *Acta Crystallogr.* **2015**, *71*, 3−8.

[5] Dolomanov, O.V.; Bourhis, L.J.; Gildea, R.J Howard, J.A.K.; Puschmann, H. OLEX2: a complete structure solution, refinement and analysis program *J. Appl. Cryst*. **2009**, *42*, 339-341.

[6] DIAMOND, Crystal and Molecular Structure Visualization Crystal Impact; Dr. H. Putz & Dr. K. Brandenburg GbR: Bonn, Germany, version 4.6.5, **2021**.